Neutron-rich B isotopes studied with antisymmetrized molecular dynamics

Yoshiko Kanada-En'yo and Hisashi Horiuchi

Department of Physics, Kyoto University, Kyoto 606-01, Japan

(Received 21 February 1995)

Structure of odd-even B isotopes up to the neutron drip line is studied systematically with the antisymmetrized molecular dynamics (AMD). The AMD method has already proved to be a powerful theoretical approach for the systematic study of nuclear structure in extensive region including exotic neutron-rich nuclei as well as ordinary nuclei. It is owing to its flexible nature free from any model assumptions such as the existence of clusters. The energies and other observed data of B isotopes are reproduced well. Especially very good reproduction of electromagnetic properties is obtained. The systematic behavior of the electromagnetic properties is explained in relation to the drastic change between clustering structure and shell-model-like structure. This explanation gives us an important indication that clustering structure in neutron-rich B nuclei is strongly suggested by the experimental data. It is shown that the structure change with increase of the neutron number is largely governed by the shell effect of neutron orbits. Exotic structure with new type of clustering is suggested to evolve in neutron-rich nuclei near the drip line.

PACS number(s): 21.10.−k, 02.70.Ns, 21.60.−n, 27.20.+n

I. INTRODUCTION

Experimental information about nuclei far from the stability line has been largely increased by means of unstable nuclear beams [1–7]. In those newly observed data, there remain many to be studied theoretically [1–4,8–10]. Our aim is to describe properties of neutron-rich nuclei consistently with the description of those of ordinary nuclei in order to understand unfamiliar properties of neutron-rich nuclei.

The recently observed data of neutron-rich B isotopes [11–13] show interesting dependence of the electric and magnetic moments on the neutron number N. It is naturally expected that the N dependence of the electromagnetic properties may be caused by some structure change such as development of clustering structure. The possibility of clustering structure in neutron-rich B isotopes has been theoretically suggested in a pioneering work [14] with the molecular-orbital model. In the model, B systems are described as being composed of an α-α core, surrounding neutrons, and a proton. It was found that the optimum α-α distance of each isotope became larger with an increase of N in the $N > 8$ region.

For theoretical research on B isotopes up to the drip line, one should take at least two essential points into account. The first point is that the traditional approaches useful for ordinary nuclei are not necessarily applicable for the study of unstable nuclei near the drip line. For example, there is little information about the effective charge to be used in the exotic region with $N \gg Z$. This point is a general problem underlying the systematic study of an extensive region containing exotic nuclei. Another point exists in the clustering aspect in light nuclei. It is well known that the cluster structure appears in some nuclei with $N \approx Z$ as seen in the $t + \alpha$ clustering of ^{7}Li and the $\alpha + \alpha$ structure of ^{8}Be [15–19]. The ordinary nucleus ^{11}B has been studied with cluster models

assuming clustering structure such as ^{7}Li$(t + \alpha) + \alpha$ [15]. However, in the case of other exotic nuclei in B isotopes, we have so little information that it is difficult to assume *a priori* the existence of some clusters in them.

In the work of this paper, we apply antisymmetrized molecular dynamics (AMD) [10,20–32] for the study of B isotopes because AMD is free from model assumptions such as the existence of clusters and the axial symmetry of the deformation. In the previous study in Ref. [10], the AMD approach has been applied to the study of the nuclear structure of Li and Be isotopes and has proved to be a very useful theoretical approach for the study of exotic nuclei near the neutron drip line as well as ordinary nuclei. In the study of Li isotopes, a very good reproduction of electromagnetic properties has been obtained and has been explained to be related to the dramatic change between clustering structure and shell-model-like structure. It has been shown that the well-developed clustering structure in ^{7}Li becomes weak as the neutron number increases and changes toward the shell-model-like structure in ^{11}Li with $N = 8$. In Be isotopes a theoretical study with the AMD method has shown two kinds of drastic structure change. One is the change from the cluster structure of ^{8}Be toward the shell-model-like structure of ^{12}Be with $N = 8$. The other is the change toward the clustering structure in the $N > 8$ region with the increase of N. What has enabled us to describe these structure changes is the flexible nature of the AMD wave function which can describe a variety of nuclear structures such as the closed-shell structure, deformed structure, and also various clustering structures. The total wave function of AMD is described by a Slater determinant of single-particle wave functions represented in the form of Gaussian wave packets. The centers of the Gaussian wave packets are considered to be variational complex parameters. The construction of energy-minimum intrinsic states is achieved by using the frictional cooling method.

Angular momentum projection is applied to these intrinsic states to obtain the eigenstates of angular momentum.

In the case of He isotopes, there have been reported extensive and successful studies by many authors, for example, by Varga et al. [33] and by Zhukov and co-workers [34,8]. Some theoretical methods of these studies are model independent like AMD. However, such theoretical methods adopted in these studies of light-mass neutron-rich nuclei are too elaborate to be extended to heavy-mass neutron-rich nuclei like boron isotopes near the neutron drip line. A great advantage of the AMD theory is that it can easily treat heavy-mass neutron-rich nuclei.

The purpose of this paper is to make a systematic study of odd-even B isotopes from ^{11}B up to ^{19}B with AMD. We expect that a drastic structure change may be seen with an increase of the neutron number N. If this is the case, one of the interesting questions is whether or not the systematic N dependence in B isotopes is similar to the one discussed in Li and Be isotopes; namely, the most shell-model-like structure appears in the nucleus with the neutron magic number $N = 8$ among the isotopes and some kind of clustering develops in the region of $N > 8$. In the case of B isotopes, there are many isotopes with $N > 8$ up to the neutron drip line isotope ^{19}B with $N = 14$. Therefore we will be able to study more about the structure change in the region beyond $N = 8$ than in the case of Be isotopes where the neutron drip line nucleus ^{14}Be has $N = 10$. The interesting N dependence of the experimental data of electromagnetic properties would be related to the systematic structure change. We will make quantitative analyses on these properties in order to understand the fundamental mechanism of the systematic structure change with neutron number. We will indicate interesting features of the structure in exotic neutron-rich B isotopes and answer the question whether or not clustering structure develops near the neutron drip line. A preliminary report of the present study was given in Ref. [24].

In Sec. II, the formulation of AMD for the study of nuclear structure is presented. We describe the wave function, the frictional cooling method, and the angular momentum projection. The two-nucleon interaction adopted in this paper is explained in Sec. III. In Sec. IV, the results of a calculation for odd-even B isotopes are compared with the data. Energy spectra and other properties such as magnetic and electric moments are found to be well reproduced. The drastic change of clustering structure with the increase of neutron number N is shown and is discussed in connection with the N dependence of the electromagnetic data. Finally, in Sec. V, summarizing discussions are given.

II. FORMULATION OF AMD

AMD is a theory which has been developed recently for the study of heavy-ion reactions [20,26–32]. The method is applicable to also nuclear structure problems [10,20–25] as well as heavy-ion collision problems. Here we only explain the AMD framework for the sake of nuclear struc-

ture studies. As for AMD theory for the sake of nuclear reaction studies, the reader is referred to Ref. [27]. Since the AMD framework for nuclear structure studies was described in detail in Refs. [10,25], here we give a brief explanation, keeping within a self-contained style.

A. Wave function of AMD

In AMD the wave function of the A-nucleon system $|\Phi\rangle$ is expressed by a Slater determinant

$$|\Phi(\mathbf{Z})\rangle = \frac{1}{\sqrt{A!}} \det[\varphi_j(i)], \quad \varphi_j = \phi_{\mathbf{Z}_j}\chi_{\alpha_j} , \quad (1)$$

where χ_{α_j} is the spin isospin wave function of the jth single-particle state labeled with $\alpha_j = p\uparrow$, $p\downarrow$, $n\uparrow$, or $n\downarrow$. The spatial wave function of the jth single-particle state $\phi_{\mathbf{Z}_j}$ is represented by a Gaussian wave packet

$$\langle \mathbf{r}|\phi_{\mathbf{Z}_j}\rangle = \left(\frac{2\nu}{\pi}\right)^{3/4} \exp\left[-\nu\left(\mathbf{r} - \frac{\mathbf{Z}_j}{\sqrt{\nu}}\right)^2 + \frac{1}{2}\mathbf{Z}_j^2\right]$$

$$\propto \exp\left[-\nu(\mathbf{r} - \mathbf{D}_j)^2 + \frac{i}{\hbar}\mathbf{K}_j \cdot \mathbf{r}\right] ,$$

$$\mathbf{Z}_j = \sqrt{\nu}\mathbf{D}_j + \frac{i}{2\hbar\sqrt{\nu}}\mathbf{K}_j , \quad (2)$$

where ν is the width of the wave packet common to all nucleons. Thus the wave function of the system $|\Phi(\mathbf{Z})\rangle$ is parametrized by the complex parameters $\{\mathbf{Z}\} = \{\mathbf{Z}_1, \mathbf{Z}_2, \ldots, \mathbf{Z}_A\}$.

For the study of nuclear structure, the AMD wave function $|\Phi(\mathbf{Z})\rangle$ explained above is projected to the parity eigenstate

$$|\Phi^{\pm}(\mathbf{Z}_1, \mathbf{Z}_2, \ldots, \mathbf{Z}_A)\rangle = (1 \pm P)|\Phi(\mathbf{Z}_1, \mathbf{Z}_2, \ldots, \mathbf{Z}_A)\rangle , \quad (3)$$

with P standing for the parity inversion operator.

The wave function $|\Phi(\mathbf{Z})\rangle$ of Eq. (1) is the same as the wave function of the fermionic molecular dynamics proposed by Feldmeier [35]. Furthermore, $|\Phi(\mathbf{Z})\rangle$ can be also regarded as a special case of the wave function of the time-dependent cluster model (TDCM) [36] where the parameters of the wave function of the Brink-type cluster model [37] are treated as time-dependent parameters by using the time-dependent variational principle. The characteristic points of the AMD method in our present approach to nuclear structure problems are that the construction of the energy-minimum intrinsic state is achieved by using the frictional cooling method and that the projection of parity and angular momentum is adopted.

B. Frictional cooling method

In order to construct the wave function $\Phi^{\pm}$ for the ground state, we should determine the parameters $\{\mathbf{Z}\}$ which minimize the expectation value of the Hamiltonian H:

$$\hat{E} = \hat{E}(\mathbf{Z}, \mathbf{Z}^*) \equiv \frac{\langle \Phi^{\pm}(\mathbf{Z})|H|\Phi^{\pm}(\mathbf{Z})\rangle}{\langle \Phi^{\pm}(\mathbf{Z})|\Phi^{\pm}(\mathbf{Z})\rangle} \ . \qquad (4)$$

First, we randomly choose parameters which express an initial state with high excitation energy. This initial state is then cooled down by applying the frictional cooling equations for $\{\mathbf{Z}\}$, expressed as

$$\frac{d\mathbf{Z}_k}{dt} = (\lambda + i\mu)\frac{1}{i\hbar}\frac{\partial \hat{E}}{\partial \mathbf{Z}_k^*} \quad \text{and c.c. ,} \qquad (5)$$

with arbitrary real numbers λ and $\mu < 0$. It is easily proved that the energy of the system decreases with time,

$$\frac{d\hat{E}}{dt} < 0 \ . \qquad (6)$$

Then the intrinsic wave function of the minimum-energy state is obtained after sufficient cooling time. This cooling method explained above is called the frictional cooling method.

C. Projection to total-angular-momentum eigenstates

The wave function of the system should be a total-angular-momentum eigenstate. For simplicity we apply the total-angular-momentum projection after the variational calculation explained above. We regard the minimum-energy state obtained with the frictional cooling method as the intrinsic state of the system. We calculate the expectation values of rank-k operators T^k with the total-angular-momentum eigenstate $|P_{MK}^J \Phi^{\pm}\rangle$, which is obtained by projecting the intrinsic wave function $|\Phi^{\pm}\rangle$,

$$\frac{\langle P_{MK}^J \Phi^{\pm}|T_{q=0}^k|P_{MK}^J \Phi^{\pm}\rangle}{\langle P_{MK}^J \Phi^{\pm}|P_{MK}^J \Phi^{\pm}\rangle} = \frac{\mathcal{T}}{\mathcal{N}} \ ,$$

$$\mathcal{T} = (JMk0|JM)\sum_{K'\nu}(JK'k\nu|JK)$$

$$\times \int d\Omega D_{K'K}^{J*}(\Omega)\langle \Phi^{\pm}|T_{\nu}^k R(\Omega)|\Phi^{\pm}\rangle \ ,$$

$$\mathcal{N} = \int d\Omega \, D_{KK}^{J*}(\Omega)\langle \Phi^{\pm}|R(\Omega)|\Phi^{\pm}\rangle \ , \qquad (7)$$

where P_{MK}^J is a total-angular-momentum projection operator,

$$P_{MK}^J \equiv \int d\Omega \, D_{MK}^{J*}(\Omega)R(\Omega) \ , \qquad (8)$$

with $R(\Omega)$ standing for the rotation operator by the Euler angle Ω. K should be chosen so as to get the minimum expectation value of the Hamiltonian in each system. K mixing, namely, the diagonalization of the Hamiltonian with respect to the K quantum number, is not made in most cases, but in some cases we show results obtained by a K-mixing calculation. The spin J of the calculated ground state has been found to be the same as the observed spin value of the ground state for every system studied here. In a practical calculation, the three-dimensional integral is evaluated numerically by taking a finite number of mesh points of the Euler angle Ω.

III. INTERACTION

For the effective interaction we have adopted case 3 of the MV1 force of Ref. [38]. The interaction MV1 force contains a zero-range three-body interaction $V_{DD}^{(e)}$ in addition to the two-body interaction part $V_{DD}^{(2)}$ which is constructed from the Volkov No. 1 force [39] by weakening the strength of its repulsive part,

$$V_{DD}^{(2)} = (1 - m + bP_{\sigma} - hP_{\tau} - mP_{\sigma}P_{\tau})\left\{V_A \exp\left[-\left(\frac{r}{r_A}\right)^2\right] + V_R \exp\left[-\left(\frac{r}{r_R}\right)^2\right]\right\} \ ,$$

$$b = h = 0 \ ,$$

$$V_A = -83.34 \text{ MeV}, \quad r_A = 1.60 \text{ fm}, \quad V_R = 104.86 \text{ MeV}, \quad r_R = 0.82 \text{ fm} \ ,$$

$$V_{DD}^{(3)} = v^{(3)}\delta(\mathbf{r}_1 - \mathbf{r}_2)\delta(\mathbf{r}_1 - \mathbf{r}_3), \quad v^{(3)} = 4000 \text{ MeV fm}^6 \ , \qquad (9)$$

where P_{σ} and P_{τ} stand for the spin and isospin exchange operators, respectively. The two-body interaction part $V_{DD}^{(2)}$ contains only Wigner and Majorana components. We have made calculations by adding appropriate Bartlett and Heisenberg components to the two-body force. However, the results have proved to be not so much affected by the additional components at least for the quantities investigated in this paper. In order to show this point explicitly, we give in Sec. IV D the electric quadrupole moments calculated by adopting $b = -0.2$ and $h = 0.4$. As for the two-body spin-orbit force V_{LS}, we have adopted the G3RS force [40] expressed as

$$V_{LS} = \{u_{\mathrm{I}}\exp(-\kappa_{\mathrm{I}}r^2) + u_{\mathrm{II}}\exp(-\kappa_{\mathrm{II}}r^2)\}P(^3O)\mathbf{L}\cdot(\mathbf{S}_1 + \mathbf{S}_2) \ ,$$

$$\mathbf{L} \equiv \mathbf{r} \times \left(-i\frac{\partial}{\partial \mathbf{r}}\right), \quad u_{\mathrm{I}} = -u_{\mathrm{II}} = 900 \text{ MeV} \ ,$$

$$\kappa_{\mathrm{I}} = 5.0 \text{ fm}^{-2}, \quad \kappa_{\mathrm{II}} = 2.778 \text{ fm}^{-2} \ , \qquad (10)$$

with **r** denoting the two-nucleon relative coordinate and with $P(^3O)$ denoting the projection operator onto the triplet odd (^3O) two-nucleon state. The Coulomb interaction is approximated by a sum of seven Gaussians following the technique of Ref. [27]. The optimum width parameter ν of wave packets is chosen for each parity of the individual system so as to get the minimum energy.

IV. RESULTS AND DISCUSSIONS

The structure of odd-even isotopes of B has been studied with AMD. The theoretical results which are calculated by projecting the AMD intrinsic wave functions with definite parity to the total-angular-momentum eigenstates are compared with the experimental data. We also analyze the intrinsic wave functions before angular momentum projection and discuss the structure of the intrinsic states.

A. Radii of nuclei

In Fig. 1, the theoretical root-mean-square radii of B isotopes are compared with the interaction radii obtained from the experimental data of the interaction cross section [5]. The optimum width parameters ν are shown in Table I. The triangles connected with the dotted line (b) indicate the AMD results with the use of the interaction parameter of the Majorana term $m = 0.576$. The extremely large radii of neutron-rich nuclei are not sufficiently reproduced with the calculations. Since the calculated radii are sensitive to the interaction, careful consideration should be made in choosing the interaction parameters such as the Majorana parameter. The solid line in Fig. 1 shows the AMD results calculated with a mass-dependent Majorana parameter: $m = 0.576, 0.576, 0.63, 0.65$, and 0.65 for ^{11}B, ^{13}B, ^{15}B, ^{17}B, and ^{19}B, re-
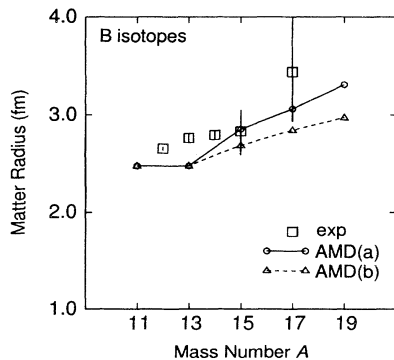

FIG. 1. Radii of B isotopes. Root-mean-square radii are calculated using the MV1 force (a) with the mass-dependent Majorana parameter described in the text and (b) with a fixed Majorana parameter $m = 0.576$. They are compared with the interaction radii derived from the data of interaction cross sections [5].

spectively. Considering that the use of larger m values for the heavier nuclear systems is generally reasonable, it is not unnatural to use the mass-dependent m values adopted here. The AMD results shown below are the ones calculated with those m values of the Majorana parameter dependent on mass number if there is no account. The results with those m values show that the neutron-rich B nuclei near the drip line have large radii considerably deviated from the $A^{1/3}$ law. As we give more detailed discussions later, the extremely large radii suggested experimentally in neutron-rich B isotopes with rather small separation energies of valence neutrons may be due to the formation of a neutron skin. The neutron skin is defined as the surface region with a rather high neutron density, but with a low proton density.

B. Binding energies and energy spectra

Figure 2 shows the binding energies of the ground states of B isotopes calculated with the MV1 force with three different choices of Majorana parameter m: $m = 0.576, 0.63$, and 0.65. It should be stressed that not the absolute values of the binding energies, but the relative binding energies between neighboring nuclei are of importance in detailed discussions on the behavior of valence neutrons, because valence neutrons can be sensitive to their separation energies.

The excitation energies of negative-parity states are shown in Fig. 3. The theoretical levels have been calculated by diagonalizing the Hamiltonian matrix with respect to the K quantum number. When the principal axis z is chosen to be the approximately axially symmetric axis in the prolate shape, the mixing of K quantum numbers is found to be small in the low-lying levels, which implies that the Hamiltonian matrix is almost diagonal with respect to the K quantum number at least for low-lying levels. We assign to each of the calculated bands the K quantum number that is just the K quantum number of the dominant component.

In ^{11}B, which has an asymmetric intrinsic deformation as shown later, the calculations show that the levels of negative-parity states are composed of a few bands with different K quantum numbers $K^{\pi} = 3/2^-, 1/2^-, 7/2^-$, and $5/2^-$. The $K^{\pi} = 3/2^-$ band contains the states with $J = 3/2_1, 5/2_1$, while the $J = 1/2_1, 3/2_2$ states are included in the $K^{\pi} = 1/2^-$ band, the $J = 7/2_1, 9/2_1$ states in the $K^{\pi} = 7/2^-$ band, and the $J = 5/2_1, 7/2_2$ states in the $K^{\pi} = 5/2^-$ band. Most of the calculated levels correspond to the observed excited states. It is found that the level spacings between adjacent band members are narrower in general than the experimental data, and it implies that the intrinsic state in each band has a rather larger moment of inertia. Since the moment of inertia is sensitive to the interaction parameters such as the Majorana parameter, it is not difficult to choose suitable interaction parameters so as to fit the observed level spacings. Another point to be discussed is concerned with the gap energies between bands. An example is the gap energy between the $K^{\pi} = 3/2^-$ and $K^{\pi} = 1/2^-$ bands, which is given by the excitation energy of the $1/2_1$

TABLE I. The optimum width parameters ν (fm^{-2}) of each system for three different values of the Majorana interaction parameter m.

Interaction	Width parameter ν (fm^{-2})				
	^{11}B	^{13}B	^{15}B	^{17}B	^{19}B
$m = 0.576$	0.185	0.175	0.175	0.165	0.160
$m = 0.63$	0.170	0.160	0.155	0.150	0.145
$m = 0.65$	-	0.155	0.150	0.150	0.135

state from the ground $3/2_1$ state. The theoretical result gives 0.4 MeV for the excitation energy, which is rather smaller than the data. The excitation energy of the $1/2_1$ state is very sensitive to the strength of the spin-orbit force. We have tried the larger strength of the LS force, $u_{\mathrm{I}} = -u_{\mathrm{II}} = 2000$ MeV instead of $u_{\mathrm{I}} = -u_{\mathrm{II}} = 900$ MeV, and have obtained 2.4 MeV excitation energy, which is as large as the experimental data. In Fig. 3 we also show the results of a calculation with other interaction parameters, $u_{\mathrm{I}} = -u_{\mathrm{II}} = 1500$ MeV and $m = 0.56$. For getting a better reproduction of the energy spectra, it is necessary to make careful consideration in choosing the interaction parameters.

We have poor experimental data in neutron-richer B isotopes. According to the AMD calculations, in ^{15}B, ^{17}B, and ^{19}B, the low-lying levels are predicted to be composed of two bands with $K^{\pi} = 3/2$ and $K^{\pi} = 1/2$. These energy spectra have close relations with the intrinsic deformation of nuclei, which we discuss in a later section.

C. Magnetic moments

Magnetic dipole moments of odd-even B isotopes calculated with AMD are not sensitive to interaction parameters like the Majorana parameter. We have checked whether the introduction of the Bartlett and Heisenberg components into the effective nuclear force affects the calculated values of the magnetic moments or not, and have found that the effects are negligibly small. In Fig. 4 it

FIG. 3. (a) Energy spectra of negative-parity states of B isotopes. Excitation energies calculated with K mixing are compared with experimental data in ^{11}B and ^{13}B. The adopted interaction is the MV1 force with $m = 0.576$ and the spin-orbit force with the strength $u_{\mathrm{I}} = -u_{\mathrm{II}} = 900$ MeV. (b) In ^{11}B, the results calculated with the interaction parameters $m = 0.56$ and $u_{\mathrm{I}} = -u_{\mathrm{II}} = 1500$ MeV are also shown.
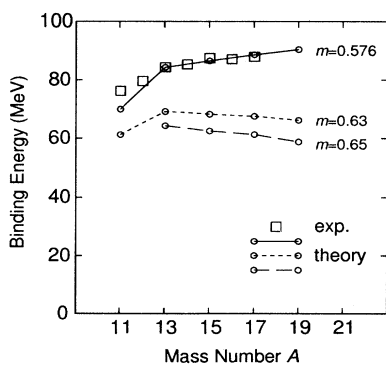
FIG. 2. Binding energies of the odd-even B isotopes calculated with the MV1 force with three different choices of the Majorana parameter $m = 0.576$, 0.63, and 0.65. Experimental data are also shown.
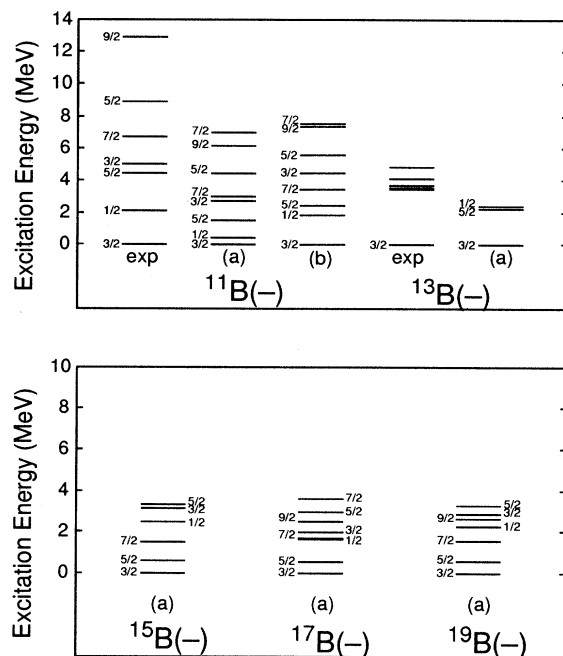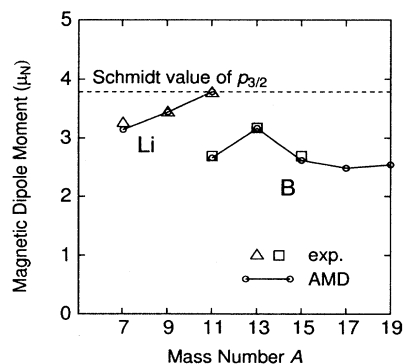
FIG. 4. Magnetic dipole moments of B isotopes. The observed data of neutron-rich nuclei ^{15}B and ^{17}B are ones obtained by the experiments with RIPS in RIKEN [11,13] (the experimental value for ^{17}B is a preliminary one). The magnetic dipole moments of Li isotopes [42,43] are also shown together with the theoretical results calculated with the AMD method.

is shown that the AMD calculations give very good reproduction of the experimental data. Furthermore, the theoretical value of the magnetic dipole moment of ^{17}B predicted with AMD has proved to agree well with the recently observed data [13]. The figure also shows the theoretical values of Li isotopes with the AMD calculations, which have been found to agree well with the experimental data in our previous paper [10].

It should be pointed out that the AMD calculations reproduce systematically the magnetic moments of B isotopes in such an extensive region that includes neutron-rich nuclei near the drip line as well as ordinary nuclei. By analyzing the AMD results, the magnetic moments of odd-even B isotopes have been found to be caused by only the proton orbits, as expected. Although B isotopes have the same proton number $Z = 5$, it is interesting that the magnetic dipole moment changes systematically with increase of the neutron number N. In Ref. [10] the N dependence of the magnetic dipole moments of Li isotopes has been discussed in relation to nuclear structure change as a function of N. Also, in the case of B isotopes, it is naturally expected that the N dependence of magnetic moments carries important information on nuclear structure. The theoretical magnetic moments of ^{17}B and ^{19}B considerably differ from the Schmidt value and suggest a clustering structure in the nuclei near the neutron drip line according to detailed discussions in the next section about the N dependence in relation to the nuclear structure.

D. Electric quadrupole moments and $B(E2)$ values

In Fig. 5, the electric quadrupole moments calculated with AMD are shown and compared with the experimental data. The solid line shows the theoretical values due to the calculation by the use of mass-dependent Majorana parameter discussed in Sec. IV A, which can give
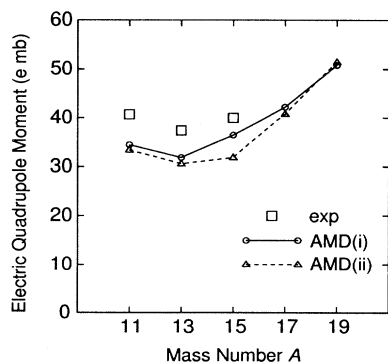

FIG. 5. Electric quadrupole moments of B isotopes. Lines are the theoretical values by AMD calculations. The solid line shows the results calculated using the mass-dependent Majorana exchange parameter. The dotted line corresponds to the results obtained by adding the Bartlett and Heisenberg components to the two-body nuclear force. Experimental data are taken from Refs. [42,12].

TABLE II. $E2$ transition strength $B(E2; I_1 \rightarrow I_2)$ in ^{11}B. Theoretical values are calculated with angular-momentum-projected AMD wave functions.

	Transition ($I_1 \rightarrow I_2$)	Energy (MeV)	Expt. ($e^2\,\mathrm{fm}^4$)	AMD ($e^2\,\mathrm{fm}^4$)
^{11}B	$5/2^- \rightarrow 3/2^-$	$4.45 \rightarrow 0$	9.6 ± 2.4	11.30
	$3/2^- \rightarrow 1/2^-$	$5.02 \rightarrow 2.13$	3 ± 0.3	6.38
	$7/2^- \rightarrow 3/2^-$	$6.74 \rightarrow 0$	1.3 ± 0.3	1.34
	$5/2^- \rightarrow 3/2^-$	$8.92 \rightarrow 0$	0.7 ± 0.5	0.05

better reproduction of radii as shown in Fig. 1. We see that the theoretical results reproduce the observed data well. It should be noted here that no effective charge is used in the AMD calculations. It is shown later that the increase of the theoretical Q moment toward the neutron drip line is due to the development of the cluster structure. We should recall that nuclei with a well-developed cluster structure may have quadrupole moments with very large absolute values because of the outer long tail of intercluster relative motion. This long tail of intercluster motion is not necessarily described in full with the present AMD wave function composed of a single parity-projected Slater determinant. We discuss this problem again in the next section.

We also show the theoretical values calculated by adopting the effective interaction with additional Bartlett and Heisenberg components in Fig. 5 (dotted line). The parameters of these components are chosen as $b = -0.2$ and $h = 0.4$. Here the Majorana parameter is chosen so as to give the same binding energies of α nuclei as the one obtained without additional components. Namely, the value of the Majorana parameter is changed from m into $m + \frac{2}{5}(b - h)$. As seen in Fig. 5, the additional Bartlett and Heisenberg components introduce no remarkable difference in the results of the electric quadrupole moments. Even in ^{15}B where the difference between two theoretical values is largest, the electric quadrupole moment of the solid line is only 5 emb larger than the one of the dotted line.

Table II shows that the $B(E2)$ values of $E2$ transitions in ^{11}B are reproduced well with the AMD calculations. It seems that the low-lying excited states are well described by the total-angular-momentum eigenstates obtained by projecting the energy-minimum intrinsic state of the AMD wave function.

V. STRUCTURE CHANGE

In the previous section, we have compared the calculated results to the experimental data. It has been found that the AMD calculations reproduce well the experimental values of various quantities which show interesting systematic dependence on the neutron number especially in the electromagnetic properties. It is important to analyze the intrinsic structure of the states obtained with AMD for a microscopic understanding of the mechanism which causes such characteristic N dependence.

A. Density distribution

As expected, a drastic structure change with the increase of the neutron number is found in the AMD intrinsic states of B isotopes. Figure 6 shows the density distributions of the intrinsic states before parity and angular momentum projection. In drawing the figures, the density of each state is projected onto the x-y plane by integrating out along the z axis perpendicular to the plane. Here the x, y, and z axes are principal axes of the deformation of the density distribution. The total matter density ρ in Fig. 6 shows the deformed state with clustering structure in ^{11}B, while the nucleus ^{13}B which has a neutron magic number $N = 8$ has the most spherical structure among B isotopes and has almost the same structure as the shell-model state. It is very interesting that in the neutron-richer nuclei ^{15}B, ^{17}B, and ^{19}B, the clustering structure with prolate deformation develops again. The intrinsic deformation increases as the neutron number goes up toward the neutron drip line. In Fig. 6 we also show a more detailed analysis by giving separately the proton density ρ_p and neutron density ρ_n. We can see a drastic structure change of the neutron density which can be explained in terms of the shell effect in neutron orbits. In ^{11}B, six neutrons have an oblate-deformed

distribution, while eight neutrons in ^{13}B constitute the closed shell and make the most spherical structure. On the other hand, ten neutrons in ^{15}B possess a large prolate deformation. It is consistent with the observed fact that ordinary nuclei with $N = 10$ such as ^{20}Ne have prolate deformation. Neutrons in ^{17}B and ^{19}B are found to have largely prolate deformed structure. The prolate structure of 14 neutrons is not an obvious feature, but is a characteristic feature seen in neutron-rich B isotopes in which 5 protons prefer prolate structure. The densities of protons ρ_p in Fig. 6 show that the structure of 5 protons in B isotopes has a similar N dependence as the neutron structure. It is seen that the clustering feature of protons appears in the nuclei ^{11}B and it becomes weaker in ^{13}B. In the neutron-richer region with $N > 8$, the proton density with two clusters stretches outward in the prolate shape. Especially well-developed clusters of proton density are seen in nuclei near the drip line. We show in Fig. 7 the density distribution of the parity-projected states $|\Phi^-(\mathbf{Z})\rangle$, which are the actual intrinsic wave functions obtained by the frictional cooling method.

For the sake of a more quantitative analysis, we introduce the values $\Delta N_p^{\mathrm{osci}}$ and $\Delta N_n^{\mathrm{osci}}$, which stand for the deviation of the proton and neutron orbits in the AMD wave function from those in the simple shell-model wave function;
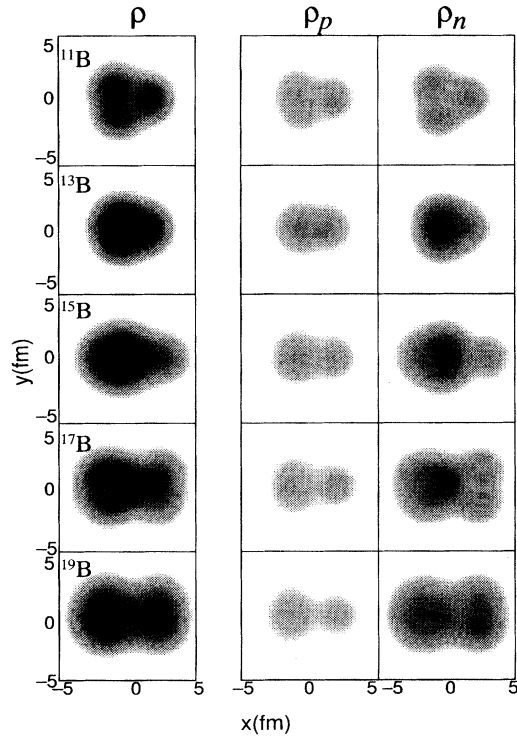

FIG. 6. Density distribution of the AMD states of B isotopes. The intrinsic matter densities ρ before parity and angular momentum projection are shown by projecting to the x-y plane with integration along the z axis perpendicular to the plane. The densities of protons ρ_p and neutrons ρ_n are also shown separately; $\rho = \rho_p + \rho_n$.
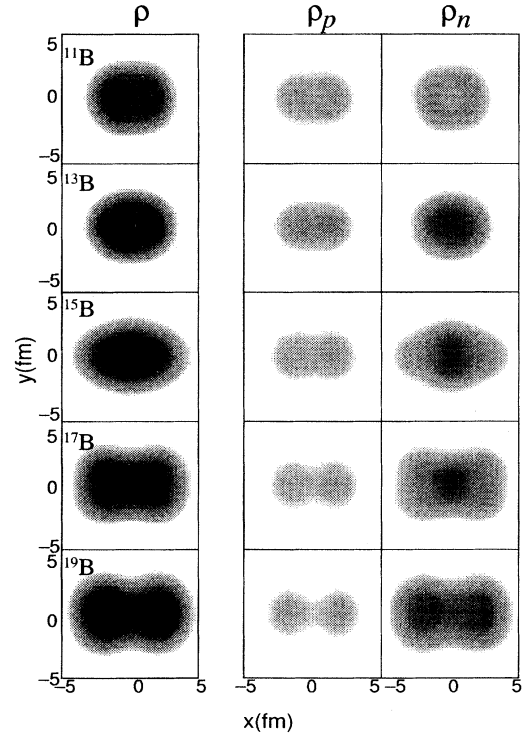
FIG. 7. Density distribution of the parity-projected AMD states of B isotopes. The intrinsic densities ρ of nuclear matter of the AMD states after parity projection are shown by projecting to the x-y plane with integration along the z axis perpendicular to the plane. The densities of protons ρ_p and neutrons ρ_n are also shown separately; $\rho = \rho_p + \rho_n$.

$$\Delta N_p^{osci} \equiv \frac{\langle P_{MK}^J \Phi^\pm | N_p^{op} | P_{MK}^J \Phi^\pm \rangle}{\langle P_{MK}^J \Phi^\pm | P_{MK}^J \Phi^\pm \rangle} - (N_p^{osci})_{\min} ,$$

$$\Delta N_n^{osci} \equiv \frac{\langle P_{MK}^J \Phi^\pm | N_n^{op} | P_{MK}^J \Phi^\pm \rangle}{\langle P_{MK}^J \Phi^\pm | P_{MK}^J \Phi^\pm \rangle} - (N_n^{osci})_{\min} , \quad (11)$$

where N_p^{op} and N_n^{op} are the oscillator quantum number operators and $(N_p^{osci})_{\min}$ and $(N_n^{osci})_{\min}$ are the minimum oscillator quantum numbers given by the simple shell model for protons and neutrons, respectively. The states with shell-model-like structure should have small values of ΔN^{osci}, while the states with a developed intrinsic deformation have large values. Figure 8 shows ΔN_n^{osci} and ΔN_p^{osci}. The value of ΔN_n^{osci} is the smallest and nearly zero in ^{13}B, which as a neutron magic number $N = 8$, and it becomes larger again as N increases in the region with $N \geq 8$. This neutron-number dependence of ΔN_n^{osci} reflects the shell effect of neutron orbits. It is seen that the ΔN_p^{osci} for proton orbits shows a similar N dependence as ΔN_n^{osci} and increases toward the neutron drip line in the $N > 8$ region. The N dependence of ΔN_n^{osci} and ΔN_p^{osci} gives us a kind of quantitative expression of the N dependence of the neutron and proton density distributions. It should be pointed out that the N dependence of proton structure originates from the shell effect of neutron orbits.

Here we discuss the neutron-skin structure, which is defined as the surface region with rather high neutron density, but with low proton density. The neutron-skin structure has been suggested to appear in such nuclei as ^{8}He and neutron-rich B isotopes in which the separation energies of the valence neutrons are a few MeV. The density distribution ρ_n of the parity-projected states in Fig. 7 shows that in neutron-rich nuclei with $N > 8$ the neutron density stretches outward and distributes widely in the outer region as the neutron number N increases. The change of neutron density is so drastic that the proton density seems to remain compact in the inner region. As a result, the neutron-rich nuclei of B isotopes have a surface region with a rather large neutron density. Figure 9 shows the density ρ_n and ρ_p of the neutrons and
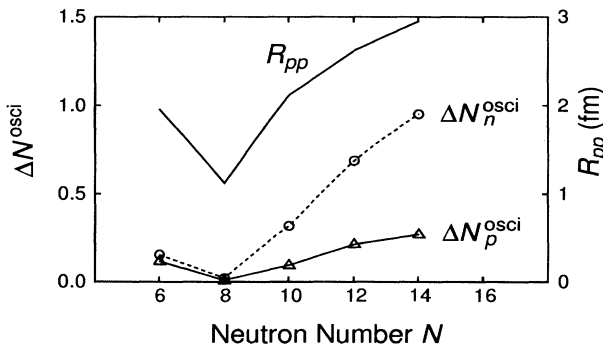

FIG. 8. Deviation of the total number of oscillator quanta of the AMD state from that of the simple-shell-model wave function. Deviation for proton orbits, ΔN_p^{osci}, and that for neutron orbits, ΔN_n^{osci}, defined in the text are shown as the function of neutron number N. The intercluster distance of proton clusters, R_{pp} (fm), is also shown.
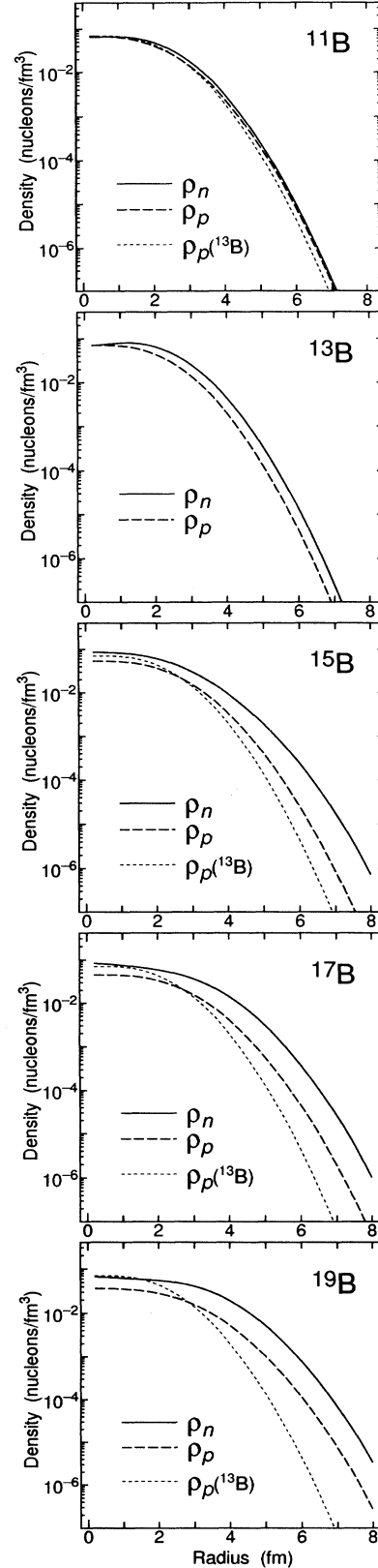

FIG. 9. Densities of neutrons $\rho_n(r)$ and protons $\rho_p(r)$ of the angular-momentum-projected states as the function of radius r (fm). ρ_n (solid lines) and ρ_p (dashed lines) of B isotopes are compared with ρ_p of ^{13}B (dotted line).

protons in the angular-momentum-projected states as a function of the radius r. The densities $\rho_n(r)$ and $\rho_p(r)$ of each B isotope are compared with the proton density of ^{13}B. In ^{11}B and ^{13}B, $\rho_n(r)$ is almost the same as $\rho_p(r)$, which is the normal property in ordinary nuclei. On the other hand, it is found that $\rho_n(r)$ in ^{15}B and ^{17}B is rather larger than $\rho_p(r)$ in the region with $r \gtrsim 3$ fm. We can estimate that the neutron skin in ^{17}B has a thickness smaller than 1 fm, which means that the neutron skin in ^{17}B is not so prominent. It is unexpected and interesting that the thickness of the neutron skin in ^{19}B is not larger than but the same as the one in ^{17}B. This is because the proton density also stretches outward following the neutron density as is seen in Fig. 6 and also in Fig. 7.

B. Clustering aspects

As mentioned in Sec. I, it is well known that some light nuclei with $N \approx Z$ have well-developed clustering structures such as the $\alpha + \alpha$ clustering of ^{8}Be and the $\alpha + t$ clustering of ^{7}Li. Even though many theoretical studies with cluster models have been made successfully, there has been a very small number of theoretical works which ascertained the formation of cluster structure microscopically without a a priori assumption of the existence of any kinds of clusters. Recently, a study with the AMD method which does not assume the existence of any kinds of clusters has assured the formation of a cluster structure in many light ordinary nuclei [25,21] and also has suggested a predominant clustering structure in the exotic nuclei of Be isotopes near the neutron drip line [10,24].

The present AMD result shows that the wave function of ^{11}B has the ^{7}Li$(\alpha + t) + \alpha$ clustering structure, which is, however, not so well developed. Furthermore, in the present AMD results, it is found that the clustering structure is prominent also in B isotopes near the drip line. Here we make detailed discussions about the clustering aspects by checking the spatial configurations of the centers of single-particle Gaussian wave packets which are expressed by the values $\{\mathbf{D}\} = \{\text{Re}\mathbf{Z}/\sqrt{\nu}\}$. Figure 10 shows the spatial configurations of $\{\mathbf{D}\} = \{\text{Re}\mathbf{Z}/\sqrt{\nu}\}$ which are projected to adequate planes. The squares and circles correspond to protons and neutrons, respectively. All even numbers of neutrons in these B isotopes couple to pairs of $n \uparrow$ and $n \downarrow$ occupying the same spatial points. It is seen that three pairs of neutrons in ^{11}B compose a triangle configuration. The configuration of four protons is almost the same as the neutron configuration, but one proton is located between two pairs of neutrons. The resulting ^{11}B structure is similar to the ^{7}Li$(\alpha + t) + \alpha$ cluster structure. In the other B isotopes except for ^{11}B, five protons are always grouped spatially into two parts as $2p + 3p$ with surrounding two groups of neutrons. In the spatial configurations in Fig. 10, clustering structures similar to ^{9}Li+α, ^{11}Li+α ^{11}Li+^{6}He, and ^{11}Li+^{8}He are seen in ^{13}B, ^{15}B, ^{17}B, and ^{19}B, respectively. We see that the relative distance between clusters increases gradually from ^{13}B to ^{19}B, which implies a systematic change from a shell-model-like structure to a
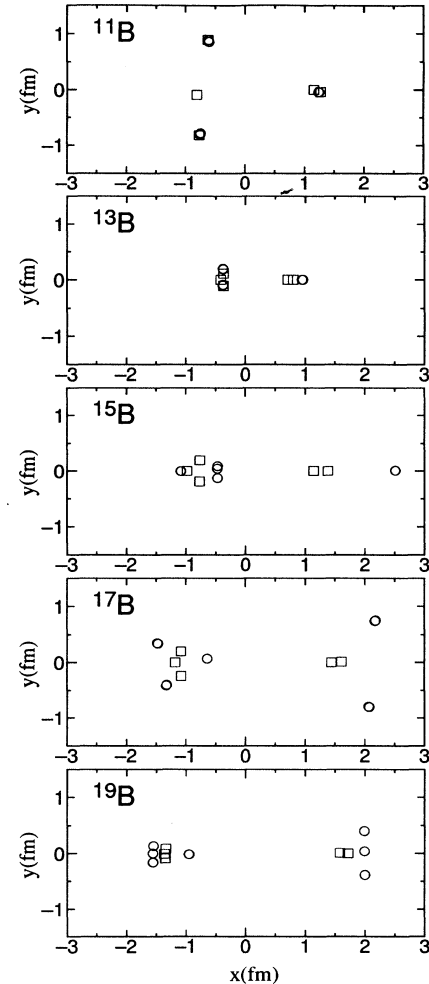

FIG. 10. Spatial configurations of the centers of nucleon wave packets expressed by $\{\text{Re}\mathbf{Z}/\sqrt{\nu}\}$ in negative-parity states of B isotopes. $\{\text{Re}\mathbf{Z}/\sqrt{\nu}\}$ are projected to an adequate x-y plane. Circles and squares represent the centers of neutrons and protons, respectively.

well-developed clustering structure. The values of inter-cluster distance show that the well-developed clustering structure is prominent in nuclei near the drip line, while in ^{13}B the shell-model-like structure is predominant. The degree of development of the clustering structure is estimated more quantitatively with the N dependence of the value R_{pp} defined as the relative distance between groups of two protons and three protons, which is almost equivalent to the intercluster distance. The calculated values of R_{pp} are given in Fig. 8. The increase of the value of R_{pp} describes quantitatively the development of cluster structure toward the drip line. The characteristic point of the clusters in the neutron-rich nuclei is that the ^{8}He-like cluster in ^{19}B, ^{6}He-like cluster in ^{17}B, and the α-like cluster in ^{15}B are not ordinary stable clusters, but somewhat distorted and polarized ones with neutrons distributing in the outer region. In the pioneering work of Ref. [14], B isotopes were studied with the molecular-

orbital model, which describes the B isotope as composed of an α-α core and surrounding proton and neutrons. It was found there that the inter-α distance increases when going from ^{13}B to ^{17}B. Their results are found to be supported by our results, which have been obtained without assuming any clusters such as the α cores.

C. Correlations of the structure
with electromagnetic properties

In the previous subsections, we have discussed the drastic change of the intrinsic structure in the region from ordinary nuclei up to the neutron-drip-line nuclei. Our purpose here is to understand the fundamental mechanism in which the observed electromagnetic properties reflect the systematic change of nuclear structure. We aim to elucidate the essential information about nuclear structure which is and will be experimentally supported. Below we discuss these problems on the basis of our AMD calculations.

We recall a previous study about Li isotopes with AMD [10], in which the N dependence of the electric and magnetic data has been explained in relation to the drastic change between the cluster and shell-model-like structures. In the following discussion, we consider two kinds of fundamental effects of cluster structure on nuclear structure which have been discussed in the previous study. One is caused by the spatial relative distance between clusters (spatial clustering), and the other is concerned with the angular momentum coupling (cluster coupling of angular momenta) caused by the clustering correlation of nucleons. As a typical example of the latter effect, we recall the so-called shell-model cluster in the SU$_3$ coupling shell-model [37,41] configuration. As

we show below, the effect of cluster structure on magnetic moments of B isotopes is made by only the cluster coupling of angular momenta, while the quadrupole moments receive both effects of the spatial clustering and the cluster coupling of angular momenta.

In order to extract the effect of the cluster coupling of angular momenta from our AMD wave functions, we have artificially made the intercluster relative distances in the AMD wave function small so as to get the shell-model limit. In practice, we have transformed all parameters $\mathbf{Z}_i$ as $\{\mathbf{Z}\} \to \{a\mathbf{Z}\}$, where a is a real constant much smaller than unity. In the state obtained in the shell-model limit, it is easily found that spatially developed clustering is not recognizable any more and that only the effect of the cluster coupling of angular momenta persists.

Table III shows the magnetic dipole moments μ and electric quadrupole moments Q calculated with the angular-momentum-projected states of the shell-model-limit intrinsic wave functions mentioned above, which are compared with the original AMD calculations. In Table III we have also shown the expectation values of the squared total angular momenta of protons $\langle \mathbf{J}_p^2 \rangle$ and neutrons $\langle \mathbf{J}_n^2 \rangle$, and those of the squared orbital angular momenta of protons $\langle \mathbf{L}_p^2 \rangle$ and of the total system $\langle \mathbf{L}^2 \rangle$. We have also shown the expectation values of the z components of the total orbital angular momenta of protons $\langle L_{pz} \rangle$ and neutrons $\langle L_{nz} \rangle$ and the z component of the total intrinsic spin of protons $\langle S_{pz} \rangle$ calculated with the highest M states $|JM\rangle = |\frac{3}{2}\frac{3}{2}\rangle$. We can see that the magnetic dipole moments in the shell-model limit are almost the same as those of the original AMD and reproduce the experimental data. This result confirms that the magnetic dipole moments are not sensitive to the relative distance between clusters; namely, the effect of clustering on the magnetic moment is not due to the spa-

TABLE III. Comparison of various quantities calculated with the AMD wave functions to those calculated with the shell-model-limit (SML) wave functions of AMD. The notations $\langle \mathbf{J}_p^2 \rangle$, $\langle \mathbf{J}_n^2 \rangle$, $\langle \mathbf{L}_p^2 \rangle$, $\langle \mathbf{L}^2 \rangle$, $\langle S_{pz} \rangle$, $\langle L_{pz} \rangle$, and $\langle L_{nz} \rangle$ are explained in the text. The experimental data of the magnetic dipole moments μ and the electric quadrupole moments Q are also shown for comparison. The expectation values are calculated with the total-angular-momentum-projected states.

		μ (μ_N)	Q (e mb)	$\langle \mathbf{J}_p^2 \rangle$	$\langle \mathbf{J}_n^2 \rangle$	$\langle \mathbf{L}_p^2 \rangle$	$\langle \mathbf{L}^2 \rangle$	$\langle S_{pz} \rangle$	$\langle L_{pz} \rangle$	$\langle L_{nz} \rangle$
^{11}B	Expt.	2.69	40							
	AMD	2.65	34.0	4.2	2.5	3.6	2.8	0.34	0.74	0.42
	SML	2.66	25.9	4.0	2.4	3.4	2.8	0.34	0.74	0.42
^{13}B	Expt.	3.17	37(4)							
	AMD	3.17	31.7	3.77	0.0	2.7	2.7	0.37	1.13	0.0
	SML	3.18	28.6	3.75	0.0	2.7	2.7	0.37	1.13	0.0
^{15}B	Expt.	2.66	38(1)							
	AMD	2.63	34.3	5.4	3.7	3.9	2.8	0.33	0.77	0.40
	SML	2.64	22.5	5.3	3.2	3.7	2.8	0.34	0.77	0.39
^{17}B	Expt.									
	AMD	2.49	42.2	5.7	4.4	4.1	2.9	0.32	0.68	0.50
	SML	2.50	22.6	5.3	4.0	3.7	2.9	0.33	0.68	0.49
^{19}B	Expt.									
	AMD	2.53	50.8	5.8	4.3	4.2	2.90	0.32	0.73	0.45
	SML	2.55	24.9	5.4	3.9	3.8	2.9	0.33	0.73	0.44
^{11}Li	Expt.	3.76	$-31(5)$							
	AMD	3.79	-29.4	3.75	0.0	2.0	2.0	0.50	1.0	0.0
	SML	3.79	-29.4	3.75	0.0	2.0	2.0	0.50	1.0	0.0

tial clustering, but due to the cluster coupling of angular momenta. More generally speaking, by comparing the original AMD results with the values in the shell-model limit, it can be confirmed that the expectation values of operators with only the linear terms of $\mathbf{J}$, $\mathbf{L}$, or $\mathbf{S}$ are determined by the cluster coupling of angular momenta predominantly.

Here we note an important point that in the calculated AMD wave functions of B isotopes, neutrons are all paired off and therefore the magnitude of the total intrinsic spin of neutrons, S_n, is 0. It implies that the total angular momentum of neutrons is exhausted by the total orbital angular momentum as $\langle \mathbf{J}_n^2 \rangle = \langle \mathbf{L}_n^2 \rangle$ and $\langle J_{nz} \rangle = \langle L_{nz} \rangle$. We have also checked that the total intrinsic spin of protons, S_p, is almost $\frac{1}{2}$, which tells us that an even number of protons are all paired off and only the intrinsic spin of the last odd proton remains in the total intrinsic spin. The total intrinsic spin $S = \frac{1}{2}$ because of $S_n = 0$ and $S_p = \frac{1}{2}$ imposes an important condition on the total orbital angular momentum L. Namely, since all B isotopes have ground states with $J = \frac{3}{2}$, only states with $L = 1$ and 2 are contained in the calculated AMD wave functions. We should remember these features of the wave functions because the following discussions are based on them.

Magnetic moments consist of two terms originating from the intrinsic spin and from the orbital angular momentum. We express the former term as μ_s and the latter term as μ_l. We need to remember that neutrons make no contribution to the calculated magnetic moments because of the pairing off of all even neutrons with $S_n = 0$, from which we have

$$\mu_s = 5.58\langle \tfrac{3}{2}\tfrac{3}{2} | S_{pz} | \tfrac{3}{2}\tfrac{3}{2} \rangle \mu_N, \quad \mu_l = \langle \tfrac{3}{2}\tfrac{3}{2} | L_{pz} | \tfrac{3}{2}\tfrac{3}{2} \rangle \mu_N , \quad (12)$$

where μ_N stands for the nuclear magneton. Figure 11 shows the two terms μ_s and μ_l and the total magnetic moments μ as a function of neutron number N. Figure 11 also shows μ_s, μ_l, and μ of Li isotopes for the sake of comparison. One of the interesting points is that the term μ_s due to the intrinsic spin is almost constant in all B isotopes, while the orbital-angular-momentum term
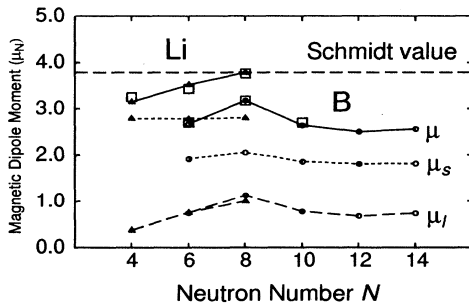
μ_l has a sizable N dependence, which indeed causes the systematic N dependence of the magnetic moment. We see a similar situation in Li isotopes: The term μ_s is almost constant for all Li isotopes, but the term μ_l has a clear N dependence which causes the N dependence of μ of Li isotopes.

Comparing the results of B and Li isotopes, we see that the magnetic dipole moments of B isotopes deviate more from the Schmidt value $3.79\mu_N$ for the $p_{3/2}$ proton orbit than those of Li isotopes. As seen in Fig. 11, since the orbital-angular-momentum terms μ_l in B isotopes are almost the same as those in Li isotopes, the essential difference of the magnetic moments between Li and B isotopes arises from the terms μ_s caused by the intrinsic proton spin. In Li isotopes the expectation value of intrinsic spin $\langle S_{pz} \rangle$ has proved to be $\langle S_{pz} \rangle = 0.5$ for all ^{7}Li, ^{9}Li, and ^{11}Li. From $\langle S_{pz} \rangle = 0.5$ we obtain $\mu_s = 2.79\mu_N$ for all Li isotopes. On the other hand, in B isotopes we have $\langle S_{pz} \rangle \approx 0.35$ as shown in Table III. From this smaller magnitude of $\langle S_{pz} \rangle \approx 0.35$, we get a smaller magnitude of $\mu_s \approx 1.8\mu_N$ for B isotopes. Below we discuss the results $\langle S_{pz} \rangle \approx 0.35$ in B isotopes and $\langle S_{pz} \rangle = 0.5$ in Li isotopes. We can get $\langle L_{pz} \rangle + \langle L_{nz} \rangle \approx 1.15$ by using the relation $\langle S_{pz} \rangle + \langle L_{pz} \rangle + \langle L_{nz} \rangle = \frac{3}{2}$. It implies that the AMD ground states of B isotopes include a component with total orbital angular momentum $L = 2$ as well as a component with $L = 1$. The inclusion of the component $L = 2$ can be also shown by calculating the magnitude $\langle \mathbf{L}^2 \rangle$. As shown in Table III, calculated values of $\langle \mathbf{L}^2 \rangle$ are 2.8, 2.7, 2.8, 2.9, and 2.9 for ^{11}B, ^{13}B, ^{15}B, ^{17}B, and ^{19}B, respectively, from which the percentage of the component $L = 2$ is easily estimated to be almost uniformly 20%. In Li isotopes $\langle S_{pz} \rangle = 0.5$ means $\langle L_{pz} \rangle + \langle L_{nz} \rangle = 1.0$, which, however, does not assure the pure $L = 1$ state. We have calculated the magnitude $\langle \mathbf{L}^2 \rangle$ and have found that $\langle \mathbf{L}^2 \rangle$ is 2.0 for all nuclei ^{7}Li, ^{9}Li, and ^{11}Li, which implies that the AMD wave functions of the Li isotopes are the pure $L = 1$ states with no mixing of the component $L = 2$.

In ^{7}Li and ^{11}Li, we can easily explain as follows why the wave functions contain purely the $L = 1$ component. Since ^{7}Li has the $\alpha + t$ cluster structure, the orbital angular momentum is carried simply by the relative motion between the clusters. The negative-parity condition in the ground state permits only the state with $L = 1$ from two possibilities of $L = 1, 2$. In ^{11}Li with the shell-model-like structure, neutrons construct a closed shell and therefore the orbital angular momentum $L = 1$ is caused by a proton in the p-shell orbit. In the case of ^{13}B, we can make a detailed analysis of the mixing of the $L = 1$ and 2 states in the AMD wave function in the shell-model limit. We give the analyses of ^{13}B and also ^{7}Li in the Appendix.

We can discuss the possible values of $\langle S_{pz} \rangle$ in Li and B isotopes if we first admit the fact that Li isotopes have pure $L = 1$ states, while B isotopes contain the mixing of the components with $L = 1$ and 2. First, in Li isotopes, by introducing the condition of $L = 1$ and $S = \frac{1}{2}$ into the relation $\langle L_z \rangle + \langle S_z \rangle = \frac{3}{2}$, we immediately obtain $\langle L_z \rangle = 1$ and $\langle S_z \rangle = \frac{1}{2}$, namely, the alignment of the intrinsic spin along the z axis. On the other hand, in B isotopes the mixing of the $L = 2$ component makes $\langle L_z \rangle > 1$, which

FIG. 11. Contributions to magnetic dipole moments μ (solid line) from the intrinsic-spin term μ_s (dotted line) and the orbital-angular-momentum term μ_l (dashed line) in both cases of Li isotopes and B isotopes. Experimental magnetic moments are also shown with squares.

causes $\langle S_z \rangle < \frac{1}{2}$. In other words, the intrinsic spin is tilted from the z axis.

As mentioned above, the N dependence of the magnetic moments is mainly due to the N dependence of the orbital-angular-momentum term μ_l. We have seen that in B isotopes $\langle L_{pz} \rangle + \langle L_{nz} \rangle$ is almost uniform, $\langle L_{pz} \rangle + \langle L_{nz} \rangle \approx 1.15$. However, each value of $\langle L_{pz} \rangle$ and $\langle L_{nz} \rangle$ is not uniform, but changes with the neutron number N. In ^{13}B the neutrons in the closed shell make $\langle L_{nz} \rangle = 0$ and in this case $\langle L_{pz} \rangle$ is largest with a magnitude about 1.15. Then $\mu_l = \langle L_{pz} \rangle \mu_N$ is largest for ^{13}B in B isotopes, resulting in the largest magnetic moments of ^{13}B. On the other hand, in other B isotopes components with the total orbital angular momentum of neutrons with $L_n \neq 0$ is mixed, which is found by analyzing the value of $\langle \mathbf{J}_n^2 \rangle = \langle \mathbf{L}_n^2 \rangle$ in Table III. The mixing of nonzero L_n components in B isotopes other than ^{13}B gives the nonzero expectation value of $\langle L_{nz} \rangle$, which generally results in the reduction of $\langle L_{pz} \rangle$ smaller than 1.15. As a result, the magnetic moments are smaller than that of ^{13}B. In this sense, what causes the N dependence of the magnetic moments is considered to be the mixing of $L_n \neq 0$ components, which must be sensitive to the neutron number N.

In summary, it has been found that the general deviation of the μ moments of B isotopes from the Schmidt value originates from the angular-momentum-coupling correlation which causes the mixing of the $L = 1$ component with the $L = 2$ component, while the N dependence originates from the coupling correlation of the orbital angular momentum of neutrons with that of protons. These correlations of the angular momentum coupling are caused by the clustering structure. Our results show that the magnetic dipole moments are not sensitive to the relative distance between clusters, but give important information on the angular momentum coupling of the clustering structure.

In contrast to magnetic dipole moments, electric quadrupole moments are sensitive to the relative distance between clusters. In the following discussion of the N dependence of the electric quadrupole moments, we try to decompose the calculated Q moments into two components: The first component is due to spatial clustering, and the second component is due to other properties of the AMD wave function including the cluster coupling of angular momenta. We consider that the second components are given by the Q moments calculated by the shell-model-limit wave functions defined above. They are shown in Table III together with the Q moments of the AMD calculations and are 25.9, 28.6, 22.5, 22.6, and 24.9 emb for ^{11}B, ^{13}B, ^{15}B, ^{17}B, and ^{19}B, respectively. These values show that the second components in the nuclei with $N \neq 8$ are smaller than the one in ^{13}B with $N = 8$. With similar argument as for μ moments, we expect that the reduction of the Q moments in B isotopes other than ^{13}B may be explained as being due to the mixing of the components with the nonzero neutron orbital angular momentum. By subtracting these second components from the total Q moments (namely, the Q moments of the AMD calculations), we can estimate the contribution of the first component due to the spatial clustering as 8.1,

3.1, 11.8, 19.6, and 25.9 emb for ^{11}B, ^{13}B, ^{15}B, ^{17}B, and ^{19}B, respectively. This component is smallest in ^{13}B and becomes larger as the neutron number increases toward the neutron drip line. Such dependence on N of the first component is indeed consistent with the drastic structure change mentioned in the previous subsection. Thus it is proved that the systematic N-dependent features of experimental data are semiquantitatively explained by the structure change given by our AMD results.

We should recall that the nucleus with a well-developed clustering structure may have a very large electric quadrupole moment due to the outer long tail of the intercluster relative motion, which cannot necessarily be described with the simple AMD wave function. In fact, the large absolute value of the quadrupole moment of ^{7}Li has been explained by improving the intercluster relative wave function of AMD calculations. It is not obvious whether or not the intercluster wave function has an outer long tail in neutron-rich nuclei with such exotic clusters that are not as stable as the normal clusters seen in ordinary nuclei. However, it is a future problem to make detailed investigations on the intercluster motion and on the possible large magnitude of the electric quadrupole moments.

VI. SUMMARY

A systematic study of the structure of odd-even B isotopes has been made with the AMD method. Radii, energy spectra, and other quantities have been reproduced rather well. An especially good reproduction of electromagnetic properties such as magnetic dipole moments and electric quadrupole moments has been obtained. It is to be stressed here that the good reproduction of the electromagnetic properties is obtained without using any effective charges and effective g factors at all.

The theoretical results have shown a drastic change of the intrinsic structure with an increase of the neutron number. The clustering structure in ^{11}B disappears and changes to the shell-model-like structure in ^{13}B. As the neutron number N increases, the clustering structure becomes prominent again in the $N > 8$ region toward the neutron drip line. Such a drastic structure change with neutron number N has been explained in connection with the shell effect in neutron orbits. We have discussed the interesting features in neutron-rich nuclei near the drip line, possible neutron-skin structure, and unfamiliar exotic clusters such as ^{6}He-like, ^{8}He-like, and ^{11}Li-like clusters. It should be noted that the clustering structure discussed here is very different from the cluster structure discussed in ordinary stable nuclei. Clusters discussed in stable nuclei are hard and difficult to be excited. But the exotic clusters discussed here such as the ^{8}He-like cluster are all soft and easy to be broken.

Systematic experimental data of the electromagnetic properties have been discussed in relation to the structure change. It has been found that magnetic dipole moments are not sensitive to the spatial clustering, but are

governed by the cluster coupling of the angular momentum. The uniform deviation of the μ moments in B isotopes from the Schmidt value for the $p_{3/2}$ proton has been explained as being due to the tilted total intrinsic spin of protons, which is caused by the mixing of the $L = 2$ component with the $L = 1$ component, while the N dependence in B isotopes has been explained as being due to the mixing of the component with the nonzero total orbital angular momentum of neutrons. In the case of the Q moments, the N dependence has been explained in terms of the two effects of the clustering structure: One is the spatial clustering, and the other is the cluster coupling of angular momenta.

There are left the problems about the effective interaction in exotic nuclei. We have tried to include a suitable amount of Bartlett and Heisenberg components into the central nuclear force in addition to Wigner and Majorana components. The electric quadrupole moments have been compared with the results without the additional components in Fig. 5. We have found that only small differences exist between these calculated results. For other quantities investigated in this paper, we could not find significant differences due to the addition of Bartlett and Heisenberg components. Thus we have assured that the Bartlett and Heisenberg components do not make much of a difference at least on the qualitative features of the nuclear structure. We have studied the effects of changing the Majorana parameter and those of omitting the density-dependence force on the calculated values of several physical quantities. The calculated results of the magnetic dipole moments have been found not to be so sensitive to the effective nuclear force, from which we can assert the reliability of our present analyses. However, some quantities such as energies and radii are sensitive to the effective interaction, and therefore it is a future problem to make detailed investigations on the choice of the interaction in order to get a better description of these quantities.

As we already mentioned, the results of our AMD study of B isotopes are quite similar to those of the previous study of Ref. [14] with respect to the structure change as a function of neutron number. It is to be noted here that some recent studies of exotic nuclei by theoretical approaches other than AMD are now giving results which are in good accordance with the AMD results. In the case of Be isotopes, the study of Ref. [45] by the use of the unrestricted Hartree-Fock method has given density distributions of ^{8}Be, ^{10}Be, ^{12}Be, and ^{14}Be which are quite similar to our AMD results of Refs. [10] and [24]; namely, ^{8}Be has α-α structure, ^{12}Be is shell-model like, and ^{14}Be has again a clustering structure. In the case of Li isotopes, the authors of Ref. [46] have adopted the microscopic multicluster model and have reproduced well the magnetic moments and electric quadrupole moments of ^{7}Li and ^{9}Li. For ^{7}Li, they adopt an $\alpha+t$ cluster configuration. Our AMD calculation has shown that the AMD wave function for ^{7}Li has just the $\alpha + t$ clustering structure. For ^{9}Li, they adopt an $\alpha + t + n + n$ four-cluster configuration and the resultant wave function is close to the harmonic-oscillator shell-model wave function except for the extreme tail region. Our AMD calculation has shown that the AMD wave function for ^{9}Li has just a structure similar to the $\alpha+t+n+n$ clustering structure, but is much closer to the shell-model wave function than in the case of ^{7}Li.

APPENDIX: SPIN COUPLING

Here we consider the single-particle wave functions

$$\varphi_i = \phi_{m_i}^{l_i}\sigma_{\mu_i}^{1/2}\tau_{\alpha_i} \quad (i = 1 - 3) , \tag{A1}$$

where τ_{α_i} is the isospin wave function with α_i standing for proton or neutron and $\sigma_{\mu_i}^{1/2}$ is the spin wave function with $\mu_i = \frac{1}{2}$ or $-\frac{1}{2}$. The spatial wave function $\phi_{m_i}^{l_i}$ is the eigenstate of the orbital angular momentum with magnitude l_i and the z component m_i. Using the relation of the angular momentum coupling,

$$|j_1m_1\rangle|j_2m_2\rangle = \sum_{|j_1-j_2|\leq J\leq j_1+j_2} \langle j_1j_2m_1m_2|JM\rangle|j_1j_2JM\rangle, \quad M = m_1 + m_2 , \tag{A2}$$

we can expand the product of the wave functions $\varphi_1\varphi_2\varphi_3$ with the total-angular-momentum eigenstates as

$$\varphi_1\varphi_2\varphi_3 = \tau_{\alpha_1}\tau_{\alpha_2}\tau_{\alpha_3}\sum_J\sum_{Ll}\sum_{Ss} C_{LS}^{JK} a_{m_1m_2m_3}^{Ll} b_{\mu_1\mu_2\mu_3}^{Ss} \left[\left[[\phi^{l_1}\phi^{l_2}]^l\phi^{l_3} \right]^L \left[[\sigma^{1/2}\sigma^{1/2}]^s\sigma^{1/2} \right]^S \right]_K^J ,$$

$$C_{LS}^{JK} = \langle LSM_LM_S|JK\rangle ,$$

$$a_{m_1m_2m_3}^{Ll} = \langle ll_3mm_3|LM_L\rangle\langle l_1l_2m_1m_2|lm\rangle ,$$

$$b_{\mu_1\mu_2\mu_3}^{Ss} = \langle s\tfrac{1}{2}\mu\mu_3|SM_S\rangle\langle \tfrac{1}{2}\tfrac{1}{2}\mu_1\mu_2|s\mu\rangle ,$$

$$m = m_1 + m_2, \quad M_L = m_1 + m_2 + m_3 ,$$

$$\mu = \mu_1 + \mu_2, \quad M_S = \mu_1 + \mu_2 + \mu_3 ,$$

$$K = M_L + M_S = m_1 + m_2 + m_3 + \mu_1 + \mu_2 + \mu_3 , \tag{A3}$$

where the notation $[\cdots]$ stands for the coupling of the angular momentum; for example, $[\phi^{j_1}\phi^{j_2}]_M^J$ represents the state with angular momentum J and its z component M, which is obtained by coupling the states ϕ^{j_1} and ϕ^{j_2}. Hence the total-angular-momentum-projected state Φ_{MK}^J of the antisymmetrized wave function $\mathcal{A}\{\varphi_1\varphi_2\varphi_3\}$ is written as

$$\Phi_{MK}^J \equiv P_{MK}^J \mathcal{A}\{\varphi_1\varphi_2\varphi_3\}$$
$$= \mathcal{A}\left\{\tau_{\alpha_1}\tau_{\alpha_2}\tau_{\alpha_3}\sum_{Ll}\sum_{Ss}C_{LS}^{JK}a_{m_1m_2m_3}^{Ll}b_{\mu_1\mu_2\mu_3}^{Ss}\left[\left[\left[\phi^{l_1}\phi^{l_2}\right]^l\phi^{l_3}\right]^L\left[\sigma^{1/2}\sigma^{1/2}\right]^s\sigma^{1/2}\right]^S\right]_M^J\right\}, \qquad (A4)$$

where P_{MK}^J is the projection operator of the total angular momentum.

We first consider the AMD wave function of ^{13}B in the shell-model limit. When we take the z axis along the principal axis with the smallest moment of inertia, $\mathbf{Z}_i$ ($i=1$–5) of protons in the AMD wave function shown in Fig. 10 are written as $(0,0,-c_1)$ and $(0,0,c_2)$ for $p\downarrow$'s and $(b,0,-c_1)$, $(-b,0,-c_1)$, and $(0,0,c_2)$ for $p\uparrow$'s, where b, c_1, and c_2 are positive constants. In the shell-model limit, in other words, in the small limit of b, c_1, and c_2, it is easily seen that the AMD wave function written as a Slater determinant of Gaussian wave packets becomes the same wave function as the shell-model wave function in which $p\downarrow$'s occupy the harmonic-oscillator orbits $(n_x,n_y,n_z)=(0,0,0)$ and $(0,0,1)$ and $p\uparrow$'s occupy the orbits $(n_x,n_y,n_z)=(0,0,0)$, $(0,0,1)$, and $(1,0,0)$. Therefore we should consider three protons in the $0p$ orbits. We need not consider neutrons because they compose the closed-shell configurations. Considering the orthogonalization of single-particle wave functions due to the antisymmetrization and the condition with $J=\frac{3}{2}$ and $K=\frac{3}{2}$ for the ground state, we can regard three protons as a $p\uparrow$ and a $p\downarrow$ in the $(lm)=(10)$ state and a $p\uparrow$ in the $(lm)=(11)$ state, namely,

$$l_1=l_2=l_3=1,\quad \alpha_1=\alpha_2=\alpha_3=p,$$

$$(m_1,m_2,m_3)=(0,0,1),\quad (\mu_1,\mu_2,\mu_3)=(\tfrac{1}{2},-\tfrac{1}{2},\tfrac{1}{2}). \qquad (A5)$$

Because of the condition $l_1=l_2=l_3=1$ and $\alpha_1=\alpha_2=\alpha_3=p$, antisymmetrization is achieved by simultaneous permutations on (m_1,m_2,m_3) and (μ_1,μ_2,μ_3). In this case Eq. (A4) can be rewritten as

$$\Phi_{MK}^J = \tau_p(1)\tau_p(2)\tau_p(3)\sum_{Ll}\sum_{Ss}C_{LS}^{JK}d_{LlSs}\left[\left[\left[\phi^1(1)\phi^1(2)\right]^l\phi^1(3)\right]^L\left[\sigma^{1/2}(1)\sigma^{1/2}(2)\right]^s\sigma^{1/2}(3)\right]^S\right]_M^J, \qquad (A6)$$

where d_{LlSs} is defined as $\mathcal{A}'\{a_{m_1m_2m_3}^{Ll}b_{\mu_1\mu_2\mu_3}^{Ss}\}$ with $\mathcal{A}'$ standing for antisymmetrization with respect to the indices (m_i,μ_i) ($i=1$–3). Then the squared amplitude of the component state with L and S in the total-angular-momentum-projected state Φ_{KM}^J is calculated as

$$\frac{\sum_{ls}|C_{LS}^{JK}d_{LlSs}|^2}{\sum_{LS}\sum_{ls}|C_{LS}^{JK}d_{LlSs}|^2}. \qquad (A7)$$

With this equation, we can show that Φ_{MK}^J with $J=\frac{3}{2}$ and $K=\frac{3}{2}$ of ^{13}B has the components of $(L,S)=(1,\frac{1}{2})$ and $(2,\frac{1}{2})$ with the squared amplitudes $\frac{5}{6}$ and $\frac{1}{6}$, respectively, from which it follows that the expectation values of $\mathbf{L}_p^2$ and $\mathbf{S}_p^2$ are 2.67 and 0.75, respectively. The expectation values of L_{pz},S_{pz} with the state Φ_{KM}^J are calculated easily by using Eq. (A6). For example, the expectation value of L_{pz} is expressed as

$$\frac{\langle\Phi_{MK}^J|L_{pz}|\Phi_{MK}^J\rangle}{\langle\Phi_{MK}^J|\Phi_{MK}^J\rangle} = \frac{\sum_{LS}\sum_{ls}|C_{LS}^{JK}d_{LlSs}|^2\sum_{M_LM_S}|\langle LSM_LM_S|JM\rangle|^2M_L}{\sum_{LS}\sum_{ls}|C_{LS}^{JK}d_{LlSs}|^2}. \qquad (A8)$$

As a result, the expectation values of L_{pz} and S_{pz} with Φ_{MK}^J $(J,M,K=\frac{3}{2},\frac{3}{2},\frac{3}{2})$ are found to be 1.13 and 0.37, respectively.

Next we consider the AMD wave function of ^{7}Li in the shell-model limit. In the case of ^{7}Li, the three nucleons in $0p$ orbits which we should consider are a $n\uparrow$ and a $n\downarrow$ in $(lm)=(10)$ and a $p\uparrow$ in $(lm)=(10)$ because the K quantum number should be chosen to be $\frac{1}{2}$ in the ground state $\Phi_{MK}^{J=3/2}$ of ^{7}Li in the AMD calculation. Using Eq. (A4) with

$$l_1=l_2=l_3=1,\quad \alpha_1=\alpha_2=n,\quad \alpha_3=p,$$

$$(m_1,m_2,m_3)=(0,0,0),\quad (\mu_1,\mu_2,\mu_3)=(\tfrac{1}{2},-\tfrac{1}{2},\tfrac{1}{2}), \qquad (A9)$$

we can show that Φ_{MK}^J with $(J,K)=(\frac{3}{2},\frac{1}{2})$ has no other component than the state with $(L,S)=(1,\frac{1}{2})$. The state of Φ_{MK}^J with $(J,K)=(\frac{3}{2},\frac{1}{2})$ with $L=1$ is composed of two states: One is the state constructed by coupling $L_n=0$

and $L_p = 1$, and the other is the state with the nonzero total orbital angular momentum of neutrons $L_n = 2$ which couples with $L_p = 1$ to $L = 1$. The total intrinsic spin of neutrons S_n is equal to 0, while that of protons S_p is $\frac{1}{2}$. With a slight modification to the calculations of the ^{13}B case, the amplitude of the components of $(L_p, L_n) = (1, 0)$ and $(L_p, L_n) = (1, 2)$ are found to be $\frac{5}{9}$ and $\frac{4}{9}$, respectively. The expectation values are obtained as $\langle \mathbf{L}_p^2 \rangle = 3.08$, $\langle \mathbf{L}_n^2 \rangle = 2.67$, $\langle \mathbf{S}_p^2 \rangle = 0.75$, and $\langle \mathbf{S}_n^2 \rangle = 0$. The expectation values of the z components of the vector operators $\mathbf{L}_p$, $\mathbf{L}_n$, and $\mathbf{S}_p$ with the state Φ_{MK}^J $(J, M, K = \frac{3}{2}, \frac{1}{2}, \frac{3}{2})$ are also easily calculated as $\langle L_{pz} \rangle = 0.33$, $\langle L_{nz} \rangle = 0.66$, and $\langle S_{pz} \rangle = 0.5$.

[1] *Proceedings of the VIth International Conference on Nuclei Far from Stability and IXth International Conference on Atomic Masses and Fundamental Constants*, Bernkastel-Kues, 1992, edited by R. Neugart and A. Wöhr, IOP Conf. Proc. No. 132 (Institute of Physics and Physical Society, London, 1993).

[2] *Proceedings of the IInd International Conference on Radioactive Nuclear Beams*, Louvain-la Neuve, 1991, edited by Th Delbar (Institute of Physics and Physical Society, London, 1992).

[3] *Proceedings of the IVth International Conference on Nucleus-Nucleus Collisions*, Kanazawa, 1991, edited by H. Toki, I. Tanihata, and H. Kamitsubo [Nucl. Phys. **A538** (1992)].

[4] *Proceedings of the International Symposium on Structure and Reactions of Unstable Nuclei*, Niigata, 1991, edited by K. Ikeda and Y. Suzuki (World Scientific, Singapore, 1992).

[5] I. Tanihata, H. Managaki, O. Hashimoto, S. Nagamiya, Y. Shida, N. Yoshikawa, O. Yamakawa, K. Sugimoto, T. Kobayashi, D. E. Greiner, N. Takahashi, and Y. Nojiri, Phys. Lett. **160B**, 380 (1985); I. Tanihata, H. Hamagaki, O. Hashimoto, Y. Shida, N. Yoshikawa, K. Sugimoto, O. Yamakawa, T. Kobayashi, and N. Takahashi, Phys. Rev. Lett. **55**, 2676 (1985); I. Tanihata, T. Kobayashi, O. Yamakawa, S. Shimoura, K. Ekuni, K. Sugimoto, N. Takahashi, T. Shimoda, and H. Sato, Phys. Lett. B **206**, 592 (1988), and references therein.

[6] W. Mittig, J. M. Chouvel, Zhang Wen Long, L. Bianchi, A. Cunsolo, B. Fernandez, A. Foti, J. Gastebois, A. Gillebert, C. Gregoire, Y. Schutz, and C. Stephan, Phys. Rev. Lett. **59**, 1889 (1987); M. G. Saint-Laurent, R. Anne, D. Bazin, D. Guillemaud-Mueller, U. Jahnke, Jin Gen Ming, A. C. Mueller, J. F. Bruandet, F. Glasser, S. Kox, E. Liatard, Tsan Ung Chan, G. J. Costa, C. Heitz, Y. El-Masri, F. Hanappe, R. Bimbot, E. Arnold, and R. Neugart, Z. Phys. A **332**, 457 (1989).

[7] T. Kobayashi, O. Yamakawa, K. Omata, K. Sugimoto, T. Shimoda, N. Takahashi, and I. Tanihata, Phys. Rev. Lett. **60**, 2599 (1988); R. Anne, S. E. Arnell, R. Bimbot, H. Emling, D. Guillemaud-Mueller, P. G. Hansen, L. Johannsen, B. Jonson, M. Lewitowitz, S. Mattsson, A. C. Mueller, R. Neugart, G. Nyman, F. Pougheon, A. Richter, K. Riisager, M. G. Saint-Laurent, G. Schrieder, O. Sorlin, and K. Wilhelmsen, Phys. Lett. B **250**, 19 (1990); M. Fukuda, T. Ichihara, N. Inabe, T. Kubo, H. Kumagai, T. Nakagawa, Y. Yano, I. Tanihata, M. Adachi, K. Asahi, M. Kouguchi, M. Ishihara, H. Sagawa, and S. Shimoura, *ibid.* **268**, 339 (1991).

[8] M. V. Zhukov, B. V. Danilin, D. V. Fedorov, J. M. Bang, I. J. Thompson, and J. S. Vaagen, Phys. Rep. **231**, 151 (1993); K. Ikeda, Nucl. Phys. **A538**, 355c (1992).

[9] T. Otsuka, N. Fukunishi, and H. Sagawa, Phys. Rev. Lett. **70**, 1385 (1993).

[10] Y. Kanada-En'yo, A. Ono, and H. Horiuchi, the preceding paper, Phys. Rev. C **52**, 628 (1995); Report No. KUNS 1320, Kyoto University, 1995.

[11] H. Okuno, K. Asahi, H. Ueno, H. Sato, M. Adachi, T. Kubo, T. Nakamura, N. Inabe, A. Yoshida, Y. Ohkubo, T. Ichihara, M. Ishihara, T. Shimoda, H. Miyatake, and N. Takahashi, Hyperfine Interact. **78**, 97 (1993).

[12] K. Asahi, H. Ueno, H. Izumi, H. Okuno, K. Nagata, H. Ogawa, Y. Hori, H. Sato, K. Mochinaga, M. Adachi, A. Yoshida, G. Liu, N. Aoi, T. Kubo, M. Ishihara, W.-D. Schmidt-Ott, T. Shimoda, H. Miyatake, S. Mitsuoka, and N. Takahashi, in Proceedings of the International Symposium on Physics of Unstable Nuclei, Niigata, 1994, edited by H. Horiuchi, K. Ikeda, K. Sato, Y. Suzuki, and I. Tanihata [Nucl. Phys. A (to be published)].

[13] H. Okuno and K. Asahi (private communication).

[14] M. Seya, M. Kohno, and S. Nagata, Prog. Theor. Phys. **65**, 204 (1981).

[15] K. Ikeda, H. Horiuchi, S. Saito, Y. Fujiwara, M. Kamimura, K. Kato, Y. Suzuki, E. Uegaki, H. Furutani, H. Kanada, T. Kaneko, S. Nagata, H. Nishioka, S. Okabe, T. Sakuda, M. Seya, Y. Abe, Y. Kondo, T. Matsuse, and A. Tohsaki-Suzuki, Prog. Theor. Phys. Suppl. **68** (1980).

[16] A. Arima, in *Nuclear Cluster Correlation, Heavy Ion Collisions*, edited by R. Bock (North-Holland, Amsterdam, 1979), Vol. 1, Chap. 3, p. 417.

[17] Y. C. Tang, *Microscopic Description of the Nuclear Cluster Theory*, Lecture Notes in Physics **145** (Springer, Berlin, 1981).

[18] V. I. Kukulin, V. G. Neudatchin, I. T. Obukhovski, and Yu. F. Smirnov, *Clusters as Subsystems in Light Nuclei, Clustering Phenomena in Nuclei* (Vieweg, Braunschweig, 1982), Vol. 3, p. 1.

[19] H. Horiuchi and K. Ikeda, *Cluster Model of the Nucleus, International Review of Nuclear Physics*, edited by T. T. S. Kuo and E. Osnes (World Scientific, Singapore, 1985), Vol. 4, pp. 1–258.

[20] H. Horiuchi, Nucl. Phys. **A522**, 257c (1991).

[21] H. Horiuchi, T. Maruyama, A. Ohnishi, and S. Yamaguchi, in *Proceedings of the International Conference on Nuclear and Atomic Clusters*, Turku, 1991, edited by M. Brenner, T. Lönnroth, and F. B. Malik (Springer, New York, 1992), p. 512; in *Proceedings of the International Symposium on Structure and Reactions of Unstable Nuclei*, Niigata, 1991, edited by K. Ikeda and Y. Suzuki (World Scientific, Singapore, 1992), p. 108.

[22] H. Horiuchi, A. Ono, Y. Kanada, T. Maruyama, and A. Ohnishi, in *Proceedings of the First Joint Italian-Japanese Meeting within the INFN-RIKEN Agreement on Perspectives in Heavy Ion Physics*, Catania, 1992, edited by M. Di Toro and E. Migneco, Conf. Proc. Vol. 38 (Italian Physical Society, Rome, 1993), p. 223.

[23] H. Horiuchi, A. Ono, and Y. Kanada-En'yo, in *Proceedings of the Seventh International Conference on Nuclear Reaction Mechanisms*, Varenna, 1994, edited by E. Gadioli [Ric. Sci. Educ. Perm. Suppl. **100**, 421 (1994)].

[24] H. Horiuchi, Y. Kanada-En'yo, and A. Ono, in *Proceedings of the Second International Conference on Atomic and Nuclear Clusters*, Santorini, 1993, edited by G. S. Anagnostatos and W. von Oertzen [Z. Phys. A **349**, 279 (1994)].

[25] Y. Kanada-En'yo and H. Horiuchi, Prog. Theory. Phys. **93**, 115 (1995).

[26] A. Ono, H. Horiuchi, T. Maruyama, and A. Ohnishi, Phys. Rev. Lett. **68**, 2898 (1992).

[27] A. Ono, H. Horiuchi, T. Maruyama, and A. Ohnishi, Prog. Theor. Phys. **87**, 1185 (1992).

[28] A. Ono, H. Horiuchi, T. Maruyama, and A. Ohnishi, Phys. Rev. C **47**, 2652 (1993).

[29] A. Ono, H. Horiuchi, and T. Maruyama, Phys. Rev. C **48**, 2946 (1993).

[30] A. Ono and H. Horiuchi, Phys. Rev. C **51**, 299 (1995).

[31] H. Horiuchi, in *Proceedings of the NATO Advanced Study Institute on Hot and Dense Nuclear Matter*, Bodrum, 1993, edited by W. Greiner, H. Stöcker, and A. Gallmann, Vol. 335 of *NATO Advanced Study Institute, Series B: Physics* (Plenum, New York, 1994), p. 215.

[32] H. Horiuchi, in *Proceedings of the Fifth International Conference on Nucleus-Nucleus Collisions*, Taormina, 1994, edited by M. di Toro, E. Migneco, and P. Piatteli [Nucl. Phys. **A583**, 297 (1995)].

[33] K. Varga, Y. Suzuki, and Y. Ohbayashi, Phys. Rev. C **50**, 189 (1994); K. Varga, Y. Suzuki, and R. Lovas, Nucl. Phys. **A571**, 447 (1994).

[34] A. A. Korsheninnikov, B. V. Danilin, and M. V. Zhukov,

Nucl. Phys. **A559**, 208 (1993).

[35] H. Feldmeier, Nucl. Phys. **A515**, 147 (1990); in *Proceedings of the NATO Advanced Study Institute on the Nuclear Equation of State*, Peñiscola, 1989, edited by W. Greiner and H. Stöcker, Vol. 216 of *NATO Advanced Study Institute, Series B: Physics* (Plenum, New York, 1989), p. 375.

[36] S. Drożdż, J. Okolowcz, and M. Ploszajczak, Phys. Lett. **109B**, 145 (1982); E. Caurier, B. Grammaticos, and T. Sami, *ibid.* **109B**, 150 (1982); Bauhoff, E. Caurier, B. Grammaticos, and M. Ploszajczak, Phys. Rev. C **32**, 1915 (1985).

[37] D. M. Brink, in *Proceedings of the International School of Physics "Enrico Fermi,"* Course XXXVI, Varenna, 1965, edited by C. Bloch (Academic, New York, 1966), p. 247.

[38] T. Ando, K. Ikeda, and A. Tohsaki, Prog. Theor. Phys. **64**, 1608 (1980).

[39] A. B. Volkov, Nucl. Phys. **74**, 33 (1965).

[40] N. Yamaguchi, T. Kasahara, S. Nagata, and Y. Akaishi, Prog. Theor. Phys. **62**, 1018 (1979); R. Tamagaki, *ibid.* **39**, 91 (1968).

[41] B. F. Bayman and A. Bohr, Nucl. Phys. **9**, 596 (1958/59).

[42] P. Raghavan, At. Data Nucl. Data Tables **42**, 189 (1989).

[43] E. Arnold, J. Bonn, R. Gegenwart, W. Neu, R. Neugart, E.-W. Otten, G. Ulm, K. Wendt, and ISOLDE Collaboration, Phys. Lett. B **197**, 311 (1987).

[44] E. Arnold, J. Bonn, W. Neu, R. Neugart, E. W. Otten, and ISOLDE Collaboration, Z. Phys. A **331**, 295 (1988); E. Arnold, J. Bonn, A. Klein, R. Neugart, M. Neuroth, E. W. Otten, P. Lievens, H. Reich, W. Widdra, and ISOLDE Collaboration, Phys. Lett. B **281**, 16 (1992).

[45] S. Takami, K. Yabana, and K. Ikeda, contribution paper to the International Symposium on Physics of Unstable Nuclei, Niigata, 1994, contribution booklet No. C-34.

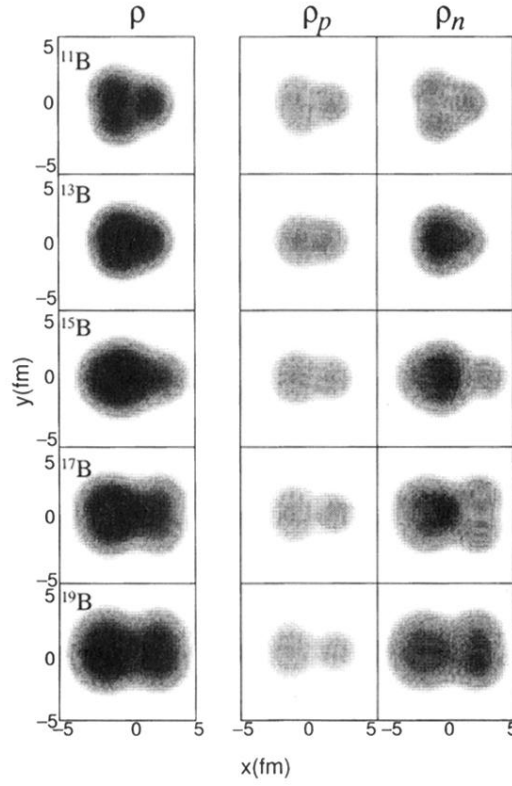[46] K. Varga, Y. Suzuki, and I. Tanihata, Report No. RIKEN-AF-NP-179, RIKEN, 1994, Phys. Rev. C (submitted).

FIG. 6. Density distribution of the AMD states of B isotopes. The intrinsic matter densities ρ before parity and angular momentum projection are shown by projecting to the x-y plane with integration along the z axis perpendicular to the plane. The densities of protons ρ_p and neutrons ρ_n are also shown separately; $\rho = \rho_p + \rho_n$.
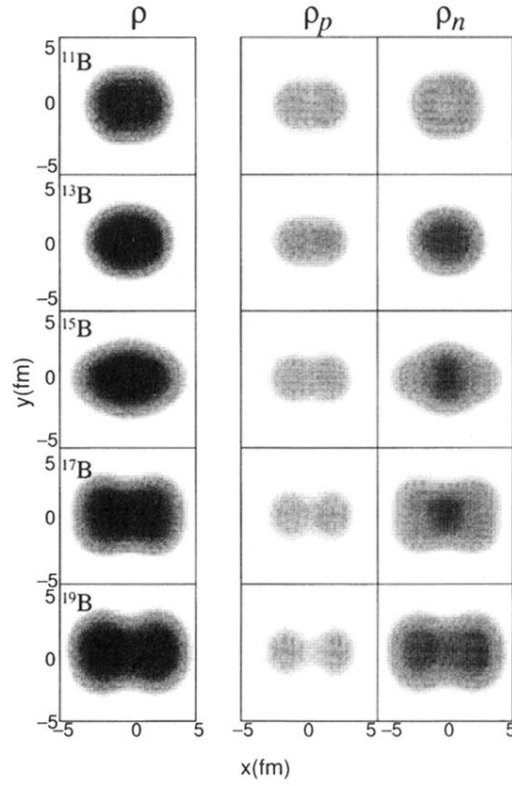
FIG. 7. Density distribution of the parity-projected AMD states of B isotopes. The intrinsic densities ρ of nuclear matter of the AMD states after parity projection are shown by projecting to the x-y plane with integration along the z axis perpendicular to the plane. The densities of protons ρ_p and neutrons ρ_n are also shown separately; $\rho = \rho_p + \rho_n$.